https://doi.org/10.1007/s41230-026-4275-9

Effects of aging process on microstructure and mechanical properties of casting Al-Si-Cu-Mg alloy

Ning Zhang[1], *Yi-cheng Feng[1,2], Ke Sun[1], Si-cong Zhao[1,2], Yuan-ke Fu[1], Lei Wang[1,2], and Ying-hu Wang[3,4]

1. School of Materials Science and Chemical Engineering, Harbin University of Science and Technology, Harbin 150040, China

2. Key Laboratory of Advanced Manufacturing and Intelligent Technology, Ministry of Education, Harbin University of Science and Technology, Harbin 150080, China

3. National Center for Materials Service Safety, University of Science and Technology Beijing, Beijing 100083, China

4. Chengdu Advanced Metallic Materials Industry Research Institute Co., Ltd., Chengdu 610300, China

Abstract: Al-Si-Cu-Mg alloy demonstrates a significant age-hardening effect, with its mechanical properties tunable by optimizing the aging parameters. To enhance this effect, the as-cast Al-8.5Si-2Cu-0.9Mg alloy was subjected to either single-stage aging at temperatures of 150 °C, 175 °C, 200 °C, and 225 °C for 0.5 h to 20 h; or double-stage aging: involving a first-stage aging treatment at 120 °C for 1 h, 3 h, 5 h, or 7 h, followed by a second-stage aging treatment at 175 °C for 0.5 h to 20 h. The microstructure and mechanical properties were evaluated for samples aged at 175 °C/7 h, 175 °C/10 h, 120 °C/5 h+175 °C/5 h, and 120 °C/5 h+175 °C/8 h. XRD analysis reveals that the as-cast Al-8.5Si-2Cu-0.9Mg alloy consists of the α-Al, Si, θ-Al_2Cu, and Q-$Al_5Cu_2Mg_8Si_6$ phases. The aging kinetics exhibit a double-peak behavior in both single-stage and double-stage aging processes. Under single-stage aging at 175 °C/*x* h and double-stage aging (120 °C/5 h+175 °C/*x* h), the precipitates' size at the first peak is smaller than that at the second peak. Compared with single-stage aging (175 °C/7 h), double-stage aging (120 °C/5 h+175 °C/5 h) produces a finer precipitate in the alloy. Theoretical calculations indicate that the number density and nucleation rate of both the $Al_5Cu_2Mg_8Si_6$ and Al_2Cu phases are higher during the double-stage aging (120 °C/5 h+175 °C/5 h) than those during the single-stage aging (175 °C/7 h). Additionally, tensile tests at both room temperature and 250 °C demonstrate that double-stage aging (120 °C/5 h+175 °C/5 h) significantly improves the mechanical properties of the alloy compared to single-stage aging (175 °C/7 h), suggesting that double-stage aging is more effective for enhancing mechanical properties for this alloy.

Keywords: casting Al-Si alloy; double-stage aging treatment; microstructure; mechanical properties

CLC numbers: TG146.21 **Document code:** A **Article ID:** 1672-6421(2026)02-223-10

1 Introduction

Al-Si alloys are widely used in aerospace, rail transit, automobile engines, and other fields due to their lightweight and high-strength[1-5]. However, the conventional Al-Si alloys are unable to maintain excellent mechanical properties at elevated temperatures[6]. Therefore, it is necessary to improve the high-temperature mechanical properties of Al-Si alloys to extend their service temperature range[7]. These properties can be enhanced through alloying with Cu and Mg, promoting the formation of thermally stable secondary phases[8-11]. Aging treatment is an effective approach to enhancing the mechanical properties of Al-Si alloys, as it can regulate the type, number density, and size of precipitates. Consequently, elucidating the effects of aging treatment on the mechanical properties of Al-Si alloys, particularly the role of Mg and Cu in the aging process, is essential for further performance optimization[12-15].

In Al-Si-Cu-Mg alloys, the aging precipitates primarily consist of Mg_2Si, Al_2Cu, and $Al_5Cu_2Mg_8Si_6$ phases[16]. Among which, the Mg_2Si and Al_2Cu phases

*Yi-cheng Feng
Male, Ph. D., Professor. His research interests focus on Al and Mg alloys.
E-mail: fyc7806067@163.com
Received: 2024-12-10; Revised: 2025-01-22; Accepted: 2025-02-19

can significantly improve the mechanical properties of the alloy at room temperature, while the $Al_5Cu_2Mg_8Si_6$ phase, a complex quaternary phase with good thermal stability, enhances the high-temperature mechanical properties of the alloy[17, 18]. However, different precipitates follow different precipitation sequences. The precipitation sequence of Mg_2Si is: SS→GP→β"→β'→β. The precipitation sequence of Al_2Cu is: supersaturation solution (SS)→pre-θ" (GP I Zone)→θ"(GP II Zone)→θ'→equilibrium θ[19]. The precipitation sequence of $Al_5Cu_2Mg_8Si_6$ is: SS→GP→Qp→Q'→Q[20]. However, the strengthening effect and precipitation behavior of different precipitates are inconsistent. Fang et al.[21] reported that in Al-Si-Cu-Mg alloys, the Q' phase exhibited a stronger aging strengthening effect compared to the θ' phase. Similarly, Xue et al.[22] conducted single-stage aging at 165 °C on Al-8Si-0.5Mg, Al-8Si-2Cu, and Al-8Si-2Cu-0.5Mg alloys. While the Qp phase demonstrated a greater rate of nucleation, the β' and θ' phases were found to exhibit a higher number density. The formation of both the θ" and Q' phases depends on the availability of Cu. When one phase precipitates preferentially, it consumes a considerable amount of Cu, thereby inhibiting the formation of the other phase. This highlights a distinct competitive relationship between the two phases during heat treatment. To promote the precipitation of the Q' phase, it is essential to first facilitate the formation of the GP zones, a process in which double-stage aging plays a pivotal role[23]. In Al-Si-Cu-Mg alloys, Cu and Mg atoms in the supersaturated Al matrix are enriched at the grain boundaries, forming the GP zones, where metastable precipitates begin to nucleate[24-26]. Zhang et al.[27] found that lower initial aging temperatures facilitated the formation of a more uniform and denser GP zone. As the aging temperature increased to 180 °C, the GP zones began to form metastable phases. The first stage of the double-stage aging treatment provided nucleation sites for metastable phase formation and resulted in high-density, uniformly distributed GP zones[28]. In summary, precipitation strengthening in Al-Si-Cu-Mg alloys is dominated by Cu partitioning competition between Al_2Cu and $Al_5Cu_2Mg_8Si_6$ precipitates, and double-stage aging enhances the strengthening by forming dense GP zones in the first stage, thereby promoting more effective precipitation during the subsequent stage. Therefore, the double-stage aging process of Al-Si-Cu-Mg alloy requires systematic investigation to elucidate the mechanisms governing the precipitation sequence, optimize processing parameters, and clarify the direct correlation between the aging process and the mechanical properties of the alloy.

To obtain an Al-Si-Cu-Mg alloy with superior comprehensive properties, both single-stage and double-stage aging processes were conducted in this study. The aging temperature and aging time at different stages were optimized, and mechanical properties of the alloy were evaluated. The effects of different aging processes on the number density and size of precipitates in Al-8.5Si-2Cu-0.9Mg alloy were analyzed to determine the optimal aging process parameters, and the mechanism of precipitation sequence was discussed. Subsequently, the Kampman-Wagner Numerical (KWN) model was employed to investigate precipitation kinetics of precipitates in different alloys. This offers significant insights for the microstructure tailoring.

2 Experimental

2.1 Experimental materials

The raw materials employed in this study were commercially pure Al (99.7wt.%), Al-20Si master alloy, Al-40Cu master alloy, Mg (99.7wt.%), Al-10Sr modifier, and Al-5Ti-1B refiner. The Al-5Ti-1B refiner and Al-10Sr modifier were added at 0.8wt.% and 0.4wt.% of the total mass of the alloy, respectively. The chemical composition of the experimental alloys is presented in Table 1. Firstly, the graphite crucible was preheated to 720±5 °C in the resistance furnace, after which commercial purity Al and an Al-Si master alloy were added. After the alloys were fully melted, the temperature was increased to 750±5 °C. Subsequently, an Al-Cu master alloy and pure Mg were added sequentially, with an interval of 10–20 min between the additions. After complete melting, the melt was refined using C_2Cl_6. Finally, the alloy melt was poured at 750 °C into a permanent mold, producing a casting with a diameter of 60 mm and a height of 120 mm. Cylindrical samples for microstructural analysis and mechanical property testing were taken from the middle and lower sections of the casting, with a sample diameter of 60 mm and a height of 20 mm.

Table1: Chemical composition of experimental alloy (wt.%)

Composition	Si	Cu	Mg	Fe	Al
Nominal	8.5	2	0.9	-	Bal.
Measured	9.2	2.4	1.1	0.08	Bal.

2.2 Solid solution treatment

The solution treatment was conducted in an SX2-4-10 type resistance furnace at a heating rate of 7 °C·min^{-1}. The samples were immediately quenched in water after removal from the resistance furnace. To determine the solution treatment temperature, the alloy was analyzed by differential scanning calorimetry (DSC, TGA/DSC3+) under an argon atmosphere. The sample was heated from 50 °C to 700 °C at a heating rate of 10 °C·min^{-1}. Figure 1(a) shows the DSC curve of as-cast Al-8.5Si-2Cu-0.9Mg alloy, revealing four endothermic peaks at 512.4 °C (Point 1), 536.1 °C (Point 2), 582.1 °C (Point 3), and 600.3 °C (Point 4). According to relevant research[29], these four endothermic peaks correspond to the melting temperatures of θ-Al_2Cu phase, Q-$Al_5Cu_2Mg_8Si_6$ phase, eutectic Si phase, and α-Al, respectively. To avoid overheating, the solution temperature should be 5–10 °C lower than the eutectic temperature of the eutectic phase with a low melting point. Considering the melting temperatures of the θ-Al_2Cu

and Q-$Al_5Cu_2Mg_8Si_6$ phases, 500 °C and 530 °C were selected as the solution temperatures. Nevertheless, the dissolution of the Q-$Al_5Cu_2Mg_8Si_6$ phase at a solid solution temperature of 500 °C remains challenging. Al-Si-Cu-Mg alloys typically undergo a two-stage solid solution treatment to overcome this challenge. According to literature[30], the solution treatment was established as 500 °C×4 h+530 °C×6 h. Figure 1(b) displays the DSC heating curve of the solution treated Al-8.5Si-2Cu-0.9Mg alloy. After solution treatment, the alloy exhibits only two endothermic peaks, appearing at 587.5 °C (Point 5) and 603.7 °C (Point 6). These peaks are associated with the melting temperatures of the eutectic Si phase and the α-Al phase, respectively. This indicates that both the θ-Al_2Cu phase with a lower melting point and the Q-$Al_5Cu_2Mg_8Si_6$ phase with a higher melting point in the Al-8.5Si-2Cu-0.9Mg alloy are completely dissolved in the Al matrix after solution treatment.

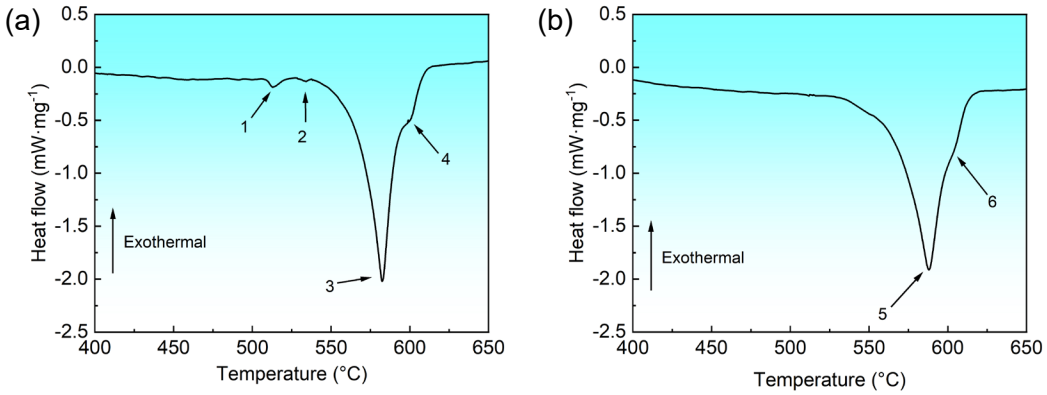

Fig. 1: DSC curves of Al-8.5Si-2Cu-0.9Mg alloy: (a) as-cast; (b) solution treatment

2.3 Aging process

The aging process was carried out after the solution treatment to promote the precipitation of strengthening phases in the Al-8.5Si-2Cu-0.9Mg alloy.

(1) Single-stage aging

To develop alloys for high-temperature applications, the aging temperature and aging time were determined based on both literature and DSC analysis[31-33]. The single-stage aging temperatures were 150 °C, 175 °C, 200 °C, and 225 °C, respectively, and the aging time was from 0.5 h to 20 h. The optimal combination of aging temperature and time under single-stage aging conditions was determined by measuring the hardness of the alloy.

(2) Double-stage aging

A double-stage aging treatment was designed to further enhance the mechanical properties of the alloy. Based on relevant literature[34-36], the first-stage aging temperature of the double-stage aging was set to 120 °C, with aging times of 1 h, 3 h, 5 h, and 7 h. The second-stage aging treatment temperature was determined based on the result of the single-stage aging treatment, and the aging times were set from 0.5 h to 20 h. The optimal double-stage aging process was identified by evaluating the hardness of the alloy.

2.4 Material characterization

Phase analysis of the sample was performed using an X-ray diffractometer (XRD, Panalytical X'PERT PRO). The Al_2Cu and $Al_5Cu_2Mg_8Si_6$ phases of the sample were characterized using a scanning electron microscope (SEM, Thermo Scientific TM Apreo C) equipped with an energy dispersive spectrometer (EDS). The precipitates of the alloy at the peak hardness condition following T6 heat treatment (single-stage and double-stage aging) were observed using a transmission electron microscope (TEM, Talo F200X). Thermo-calc software was used to simulate the number density and size of the precipitates after single-stage and double-stage aging.

2.5 Mechanical properties testing

The Vickers hardness of the samples was measured using an HXD-1000 digital microhardness tester, under a load of 100 g and holding for 15 s. Six indentations were measured on each sample, and the average value was taken as the final result. The tensile properties of the experimental alloy were measured using an MTS hydraulic electronically controlled universal testing machine. The dimensions of the tensile specimens are shown in Fig. 2. The tensile rate was set at 1 mm·min^{-1}, and three specimens were tested from each group. The final result was obtained by averaging the measurements from three samples.

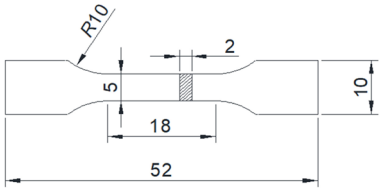

Fig. 2: Dimension of the tensile specimens (mm)

3 Results

3.1 Microstructure

The XRD pattern of the as-cast Al-8.5Si-2Cu-0.9Mg alloy is shown in Fig. 3. Diffraction peaks corresponding to the α-Al, Si, θ-Al_2Cu, and Q-$Al_5Cu_2Mg_8Si_6$ phases are identified. Figure 4(a) presents the SEM image of the as-cast Al-8.5Si-2Cu-0.9Mg alloy, revealing the presence of both reticular and block phases. Figure 4(b) presents a high-magnification SEM

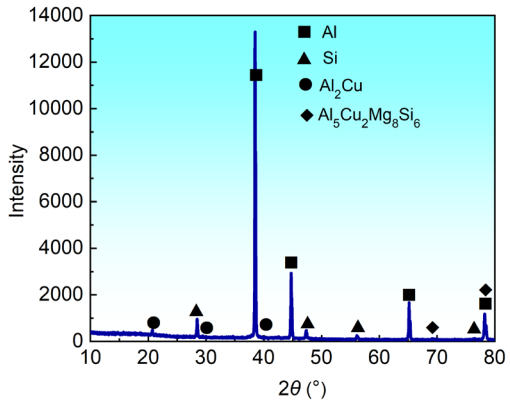

Fig. 3: XRD pattern of Al-8.5Si-2Cu-0.9Mg alloy

image of the alloy, with EDS used to analyze the bright blocky, bright reticular, and gray block phases, as summarized in Table 2. As shown in Table 2, the Al_2Cu precipitates within the alloy exhibit two distinct morphologies: reticular and blocky. The gray block phase is speculated to be the Q-$Al_5Cu_2Mg_8Si_6$ phase. As shown in Fig. 4(c), the Si element in the alloy mainly exists in eutectic Si and the Cu element is enriched in the Al_2Cu phase. Furthermore, the Q-$Al_5Cu_2Mg_8Si_6$ phase is characterized by an enrichment of Cu, Mg, and Si elements.

Figure 5 shows the SEM images of the Al-8.5Si-2Cu-0.9Mg alloy after solution treatment at 500 °C×4 h+530 °C×6 h, along with the corresponding element distribution maps. Figures 5(a) and (b) reveal that the eutectic Si is spheroidized, and that

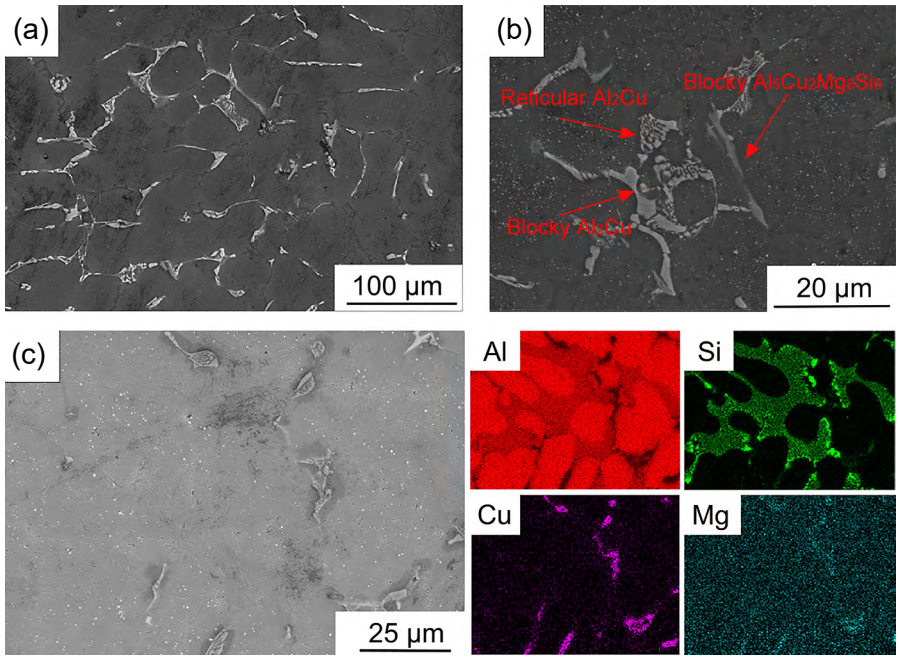

Fig. 4: SEM image of as-cast Al-8.5Si-2Cu-0.9Mg alloy and the corresponding elemental mapping: (a) low magnification; (b) high magnification; (c) the corresponding elemental mapping

Table 2: Chemical composition of intermetallic compounds in as-cast alloys by EDS point analysis (at.%)

Regions	Si	Cu	Mg	Al
Blocky Al_2Cu	2.77	27.13	0.32	69.78
Reticular Al_2Cu	1.37	26.35	0.72	71.56
Blocky Q-$Al_5Cu_2Mg_8Si_6$	22.35	8.75	24.42	44.48

some $Al_5Cu_2Mg_8Si_6$ phases persist after solution treatment. Figure 5(c) displays the SEM image and corresponding EDS mappings of the Al-8.5Si-2Cu-0.9Mg alloy after solution treatment, demonstrating that Cu and Mg are uniform in Al matrix.

3.2 Aging hardness

Figure 6 shows the age-hardening curves of the solution-treated Al-8.5Si-2Cu-0.9Mg alloy after single-stage and double-stage aging treatments. In single-stage aging [Fig. 6(a)], as the aging temperature increases, the time required for the alloy's hardness to reach its first peak decreases. The aging time for the first peak at the aging temperatures of 150 °C, 175 °C, 200 °C, and 225 °C is 10 h, 7 h, 5 h, and 2 h, respectively. The maximum hardness is achieved with single-stage aging at 175 °C for 7 h. Under this conditions, the second peak occurs at 10 h. In the single-stage aging, the double-peak phenomenon is not observed at 150 °C, probably because the relatively low temperature does not provide sufficient driving force for phase transformation, thereby restricting further precipitate evolution. According to the first peak hardness, the second-stage temperature for the double-stage aging was set at 175 °C.

The aging hardness curve of Al-Si-Cu-Mg alloy after double-stage aging is shown in Fig. 6(b). As the first-stage aging time increases, the first hardness peak shifts to longer aging times and the second peak shifts to earlier aging times, resulting in a reduced interval between the two peaks. The hardness value is the highest when the double-aging is 120 °C/5 h+175 °C/5 h, demonstrating that an optimized aging process can enhance

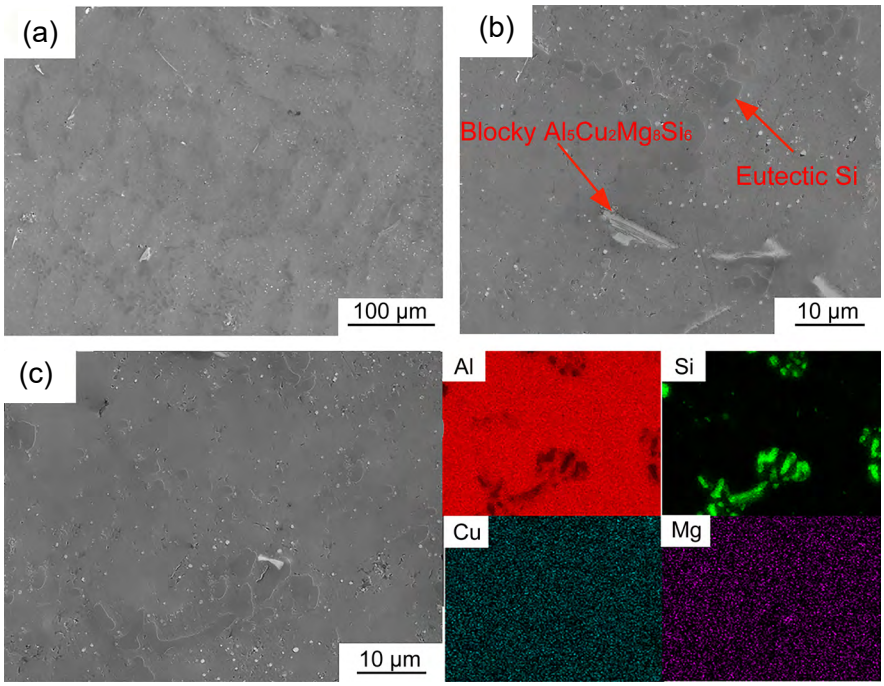

Fig. 5: SEM images of solution treatment Al-8.5Si-2Cu-0.9Mg alloy and related element distribution mappings: (a) low magnification; (b) high magnification; (c) the corresponding elemental mapping

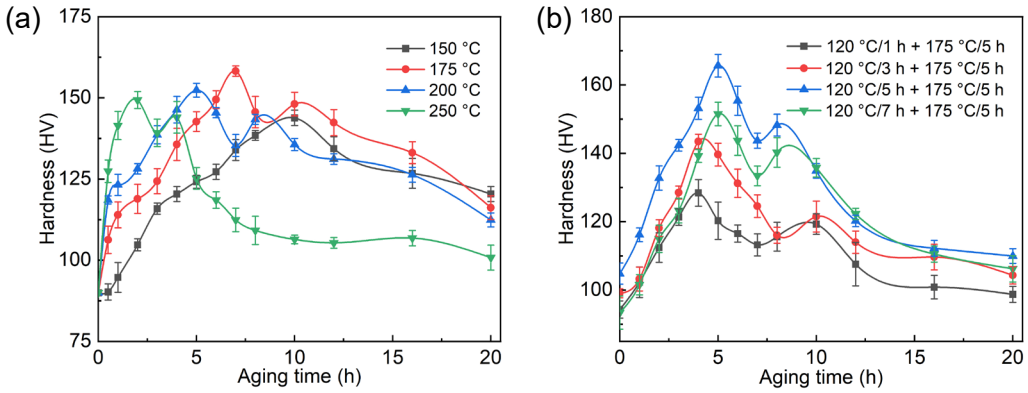

Fig. 6: Aging hardening curves of Al-8.5Si-2Cu-0.9Mg alloy at different temperatures and times: (a) single-stage aging; (b) double-stage aging

its hardness. In double-stage aging, the first-stage treatment promotes the formation of numerous fine and uniform initial precipitates (e.g., GP zones), allowing the subsequent high-temperature aging process to primarily rely on the growth and transformation of these initial phases, rather than on direct precipitation from the solid solution. Extending the second-stage aging time (e.g., to 7 h) may result in excessive growth or roughening of the precipitates, thus diminishing the reinforcement effect. Among them, the peak hardness of double-stage aging of 120 °C/1 h+175 °C/4 h and 120 °C/3 h +175 °C/4 h is lower than that of single-stage aging at 175 °C, presumably because the pre-aging time is too short to generate sufficient precipitates. Whereas for 120 °C/7 h+175 °C/5 h, excessive pre-aging likely reduces the available solute supersaturation and accelerates precipitate evolution during the second stage, thereby promoting over-aging and lowering the peak hardness relative to single-stage aging at 175 °C. The two hardness peaks reflect a sequential strengthening associated with the precipitation/transformation of different precipitates, with a transient softening stage caused by precipitate coarsening.

To further investigate the effects of the aging conditions on the precipitates of the alloy, TEM was used to observe the microstructures of the Al-8.5Si-2Cu-0.9Mg alloy at the peak aging states under both single-stage and double-stage aging conditions. Figure 7(a) shows a significant number of round disc-shaped and granular precipitates. According to Ref. [37], the round disc-shaped phase is identified as the metastable θ″ phase, which forms from the growth of the GP zone during the aging process. Its lattice constants are a=6.07 Å and c=4.87 Å according to the electron diffraction spot in Fig. 7(e). The granular phase is identified as the Q′ phase, with lattice constants of a=10.32 Å and c=4.05 Å according to the electron diffraction spot in Fig. 7(f). TEM images obtained from single-stage aging (175 °C/7 h or 175 °C/10 h) and double-stage aging (120 °C/5 h+175 °C/5 h and 120 °C/5 h+175 °C/8 h) of

the alloy were quantitatively analyzed [Figs. 7(a)–(d)]. The sizes of precipitates are summarized in Table 3. Under single-stage aging, the size of the precipitates at 175 °C/7 h aging treatment is smaller than that at 175 °C/10 h. Similarly, under double-stage aging, the size of the alloy precipitates at 120 °C/5 h+175 °C/5 h aging treatment is smaller than that at 120 °C/5 h+175 °C/8 h. As aging time increases, precipitates coarsen while their number diminishes, reducing their capacity to impede dislocation movement and thereby weakening their pinning effect. Consequently, the alloy's hardness at the second aging peak is lower than at the first peak.

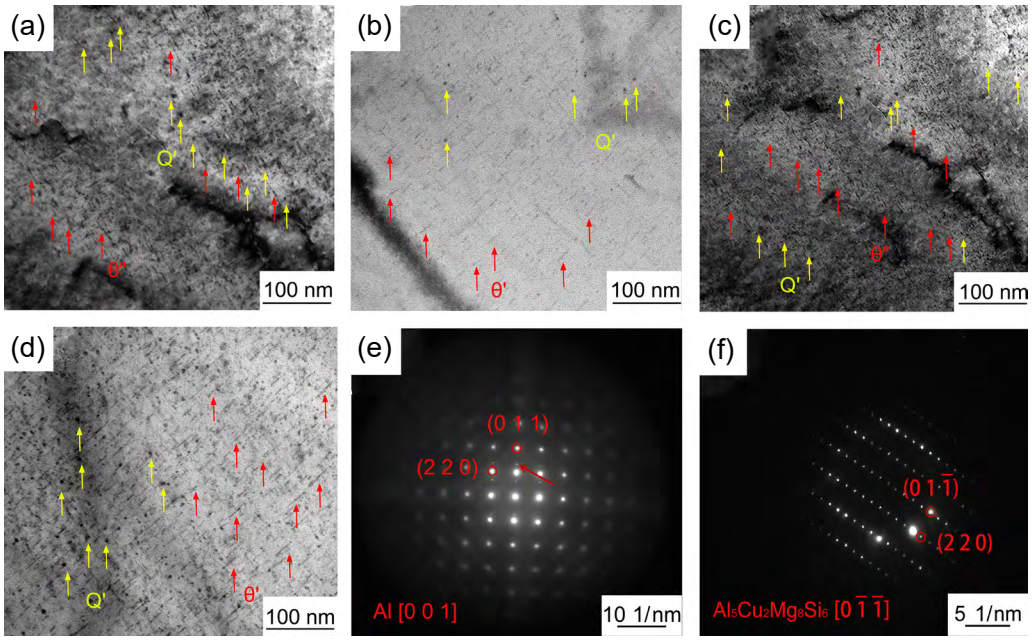

Fig. 7: TEM bright field images and selected area electron diffraction (SAED) pattern of Al-8.5Si-2Cu-0.9Mg alloy under single-stage aging and double-stage aging: (a) 175 °C/7 h; (b) 175 °C/10 h; (c) 120 °C/5 h+175 °C/5 h; (d) 120 °C/5 h+175 °C/8 h; (e) θ″ phase electron diffraction spots; (f) Q′ phase electron diffraction spots

Table 3: Statistical results of alloy precipitates under different aging processes

Process	Precipitates type	Diameter (nm)	Thickness (nm)
175 °C/7 h	θ"	19.22	2.01
	Q'	5.92	/
175 °C/10 h	θ'	23.32	3.82
	Q'	8.56	/
120 °C/5 h+ 175 °C/5 h	θ"	17.98	1.54
	Q'	5.64	/
120 °C/5 h+ 175 °C/8 h	θ'	22.42	3.55
	Q'	6.45	/

3.3 Tensile property

As shown in Fig. 8, the tensile properties of the Al-Si-Cu-Mg alloy were evaluated after four aging treatments: 175 °C/7 h, 175 °C/10 h, 120 °C/5 h+175 °C/5 h, and 120 °C/5 h+175 °C/8 h. Under single-stage aging, the room temperature tensile strength of the alloy aged at 175 °C/7 h is higher than that at 175 °C/10 h, whereas its high-temperature tensile strength is lower. Similarly, under double-stage aging, the room temperature tensile strength of the alloy aged at 120 °C/5 h+ 175 °C/5 h is also higher than that of the alloy aged at 120 °C/5 h+175 °C/8 h, while its high-temperature tensile strength is lower.

At room temperature, the Al-8.5Si-2Cu-0.9Mg alloy aged at 175 °C/7 h exhibits a yield strength of 272.6 MPa, an ultimate tensile strength of 348.9 MPa, and an elongation of 3.8%. The yield strength and ultimate tensile strength of the 175 °C/10 h aged alloy decrease to 242.5 MPa and 307.5 MPa, respectively, while the elongation increases slightly to 4.2%. When subjected to a double-stage aging treatment (120 °C/5 h+175 °C/5 h), the alloy exhibits increased yield and ultimate tensile strengths compared to single-stage aging at 175 °C/7 h, although its elongation decreases. Specifically, under the double-stage aging treatment (120 °C/5 h+175 °C/5 h), the yield strength, ultimate tensile strength, and elongation are 278.1 MPa, 359.4 MPa, and 3.1%, respectively. Moreover, the yield strength and ultimate tensile strength of the alloy aged at 120 °C/5 h+175 °C/8 h decrease to 260.3 MPa and 325.5 MPa, respectively, compared to the alloy aged at 175 °C/7 h, while the elongation increases to 5.5%. At a tensile temperature of 250 °C, the yield strength, ultimate tensile strength, and elongation of Al-8.5Si-2Cu-0.9Mg alloy aged at 175 °C/7 h are 148.5 MPa, 174.3 MPa, and 6.7%, respectively. At the same temperature, the yield strength and tensile strength of the alloys aged at 175 °C/10 h, 120 °C/5 h+175 °C/5 h and 120 °C/5 h+ 175 °C/8 h are all higher than those obtained at 175 °C/7 h. Furthermore, the alloy aged at 120 °C/5 h+175 °C/8 h exhibits the highest yield strength and ultimate tensile

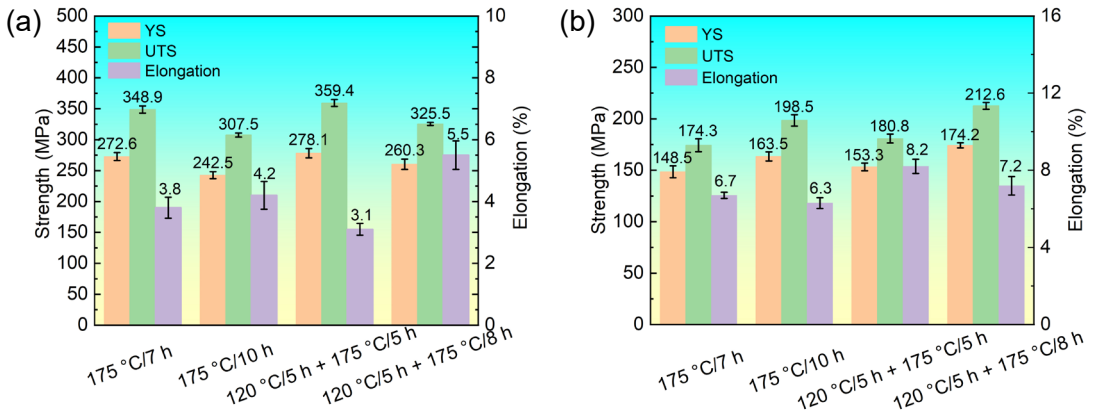

Fig. 8: Tensile properties of Al-8.5Si-2Cu-0.9Mg alloy after different aging treatments: (a) room temperature; (b) 250 °C

strength at 250 °C, reaching 174.2 MPa and 212.6 MPa, respectively.

4 Discussion

4.1 Simulation of solidification process and precipitation evolution

Figure 9(a) illustrates the intermetallic compounds formed during the solidification of Al-8.5Si-2Cu-0.9Mg alloy. The alloy is composed of α-Al, Si, Al_2Cu, and $Al_5Cu_2Mg_8Si_6$ phases, consistent with the experimental results. Among these, the Al_2Cu and $Al_5Cu_2Mg_8Si_6$ phases are the aging precipitates. To analyze the effect of aging process on the nucleation rate of the precipitates, the variation curve of the number density of the precipitates in the alloy with time under single-stage aging at 175 °C was calculated, as shown in Figs. 9(b) and (c). According to the classic Kampmann-Wagner Numerical (KWN) model, the evolution of the number density of homogeneously nucleated precipitates is expressed by Eq. (1)[38]:

$$\frac{\mathrm{d}N}{\mathrm{d}t} = N_0 Z\beta^* \exp\left(-\frac{\Delta G}{K_B T}\right)\exp\left(-\frac{\tau}{t}\right) \quad (1)$$

where N_0 is the number density of potential nucleation sites for precipitation; Z is the Zeldovich factor; β^* is the atomic impingement rate; K_B is the Boltzmann constant; τ is the incubation time for nucleation; and ΔG is the nucleation activation energy of heterogeneous nucleation. The corresponding activation energy for nucleation is[38]:

$$\Delta G = \frac{16}{3}\pi\frac{\gamma^3}{\Delta g^2} \quad (2)$$

where γ is the interface energy of the precipitate nucleus; Δg is the driving force for nucleation. Among them, the $Al_5Cu_2Mg_8Si_6$ phase exhibits a faster nucleation rate, which is mainly due to the higher interface energy between the Al_2Cu phase and the matrix (γ=0.49).

The time-dependent evolution of precipitate number density during double-stage aging (120 °C/5 h+175 °C/5 h) is illustrated in Figs. 9(e) and (f). The number density and nucleation rate of Al_2Cu and $Al_5Cu_2Mg_8Si_6$ phases under double-stage aging are higher than that under single-stage aging. Moreover, under both single-stage and double-stage aging, the number density of the Al_2Cu phase in the alloy is higher than that of $Al_5Cu_2Mg_8Si_6$ phase. The 120 °C/5 h+175 °C/8 h condition is not included in the simulations, as the analysis aims to isolate the nucleation conditions established during low-temperature pre-aging (120 °C). Prolonging the second stage aging time from 5 h to 8 h mainly affects precipitates growth/coarsening, which is outside the scope of the present study. Figure 9(d) shows the Gibbs free energy of Al_2Cu and $Al_5Cu_2Mg_8Si_6$ phases in Al-8.5Si-2Cu-0.9Mg alloy at different temperatures. The Gibbs free energy of Al_2Cu and $Al_5Cu_2Mg_8Si_6$ phases at 158 °C is equal. When low-temperature aging is performed at 120 °C, the Gibbs free energy of the $Al_5Cu_2Mg_8Si_6$ phase is lower, making its formation more favorable.

The driving force of nucleation can be written as[38]:

$$\Delta g = -\frac{kT}{v_{at}}\ln\left(-\frac{C}{C_{eq}}\right) \quad (3)$$

where v_{at} is the atomic volume, T is the absolute temperature, C_{eq} is the equilibrium solute concentration of the matrix, and C is the current solute concentration of the matrix. Compared with single-stage aging, the first-stage aging of double-stage aging is conducted at low temperatures (T=120 °C), where the solute diffusion rate is slower, suppressing precipitate growth/coarsening and favoring the formation of more and finer GP zones. As time goes on, the solute supersaturation is progressively consumed, and the driving force for nucleation decreases. Therefore, the excessive driving force caused by single-stage aging and the formation of coarser precipitates are avoided.

In the classical Kampmann-Wagner Numerical (KWN) model, the growth rate is described by the following Eq. (4)[22]:

$$\frac{\mathrm{d}r}{\mathrm{d}t} = \frac{D_i}{r}\frac{C_i^m - C_i^{inter}}{C_i^p - C_i^{inter}} \quad (4)$$

where, r is the radius of the spherical precipitate, D_i is the diffusion rate, C_i^p and C_i^m are the concentration of the solute element in the precipitate and matrix, respectively, and the concentration of the solute element at the precipitate/matrix interface is C_i^{inter}. From Eq. (4), it is evident that the growth rate depends on the diffusion rate of the slowest element. The diffusion rates of Si, Mg, and Cu are in the order of

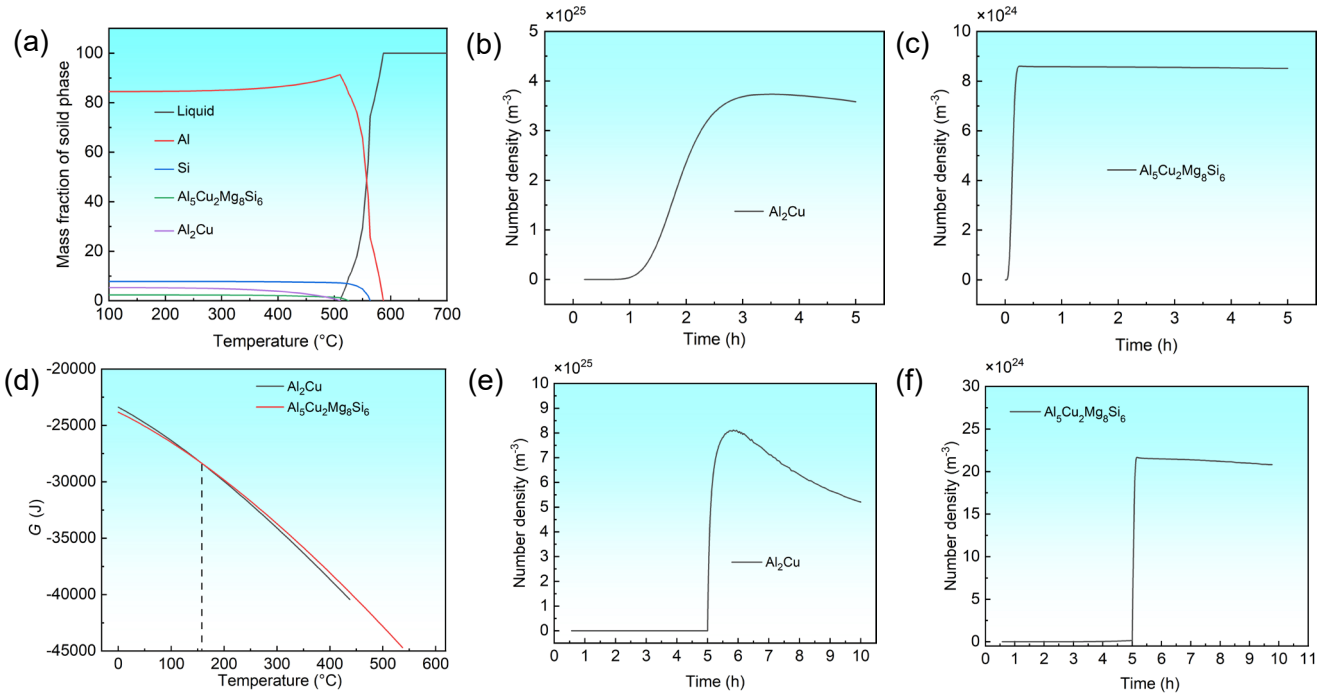

Fig. 9: Thermodynamic calculation of Al-8.5Si-2Cu-0.9Mg alloy: (a) solidification process; (b) change of number density of Al_2Cu phase with time after single-stage aging at 175 °C; (c) change of number density of $Al_5Cu_2Mg_8Si_6$ phase with time after single-stage aging at 175 °C; (d) change of Gibbs free energy of Al_2Cu and $Al_5Cu_2Mg_8Si_6$ phase with temperature; (e) change of number density of Al_2Cu phase with time after double-stage aging at 120 °C/5 h+175 °C/5 h; (f) change of number density of $Al_5Cu_2Mg_8Si_6$ phase with time after double-stage aging at 120 °C/5 h+175 °C/5 h

D_{Mg} (3.64×10^{-21} $m^2\cdot s^{-1}$)>D_{Si} (3.13×10^{-21} $m^2\cdot s^{-1}$) >D_{Cu} (1.99×10^{-21} $m^2\cdot s^{-1}$)[22]. Therefore, the growth rates of both the Al_2Cu phase and $Al_5Cu_2Mg_8Si_6$ phase are limited by the diffusion rate of the Cu element. When the diffusion rate is constant, the radius of the precipitates and the concentration difference of Cu in the solid solution are the primary factors influencing the growth rate of the precipitate phase. To analyze the variation in solute concentration difference during precipitate growth, the change in solid solution concentration with respect to precipitate radius was theoretically calculated using the classical KWN model. In the simulation, the interfacial energies of Qp/α-Al and θ'/α-Al were 0.19 $J\cdot m^{-2}$ and 0.49 $J\cdot m^{-2}$, respectively[39]. The aspect ratios of the θ' and Q' phases were 20:1 and 1, respectively. Figure 10 shows the contour diagram of the solid solution concentration versus the precipitate radius. The growth rates of the Al_2Cu and $Al_5Cu_2Mg_8Si_6$ phases, measured at an equivalent precipitate radius of 6 nm, were 3.95×10^4 $nm\cdot s^{-1}$ and 2.45×10^4 $nm\cdot s^{-1}$ under single-stage aging at 175 °C/7 h, and 3.91×10^4 $nm\cdot s^{-1}$ and 2.38×10^4 $nm\cdot s^{-1}$ under double-stage aging at 120 °C/5 h+ 175 °C/5 h, respectively. Under double-stage aging (120 °C/5 h +175 °C/5 h), the growth rates of the Al_2Cu and $Al_5Cu_2Mg_8Si_6$ phases are slightly lower than those observed under single-stage aging (175 °C/7 h), primarily due to the low-temperature stage, which reduces the solute concentration in the matrix and consequently limits the growth rate of precipitates.

4.2 Influence of precipitation strengthening on mechanical properties

Changes in tensile properties are attributed to changes in the quantity and size of Al_2Cu and $Al_5Cu_2Mg_8Si_6$ phases, which can be described by the Orowan strengthening mechanism[40]:

$$\Delta\sigma=\frac{MGb}{2\pi\sqrt{1-\nu}}\left(\frac{1}{1.123d\sqrt{\frac{0.318\pi}{af}}-\frac{\pi d}{8}-\frac{1.061d}{a}}\right)\ln\frac{0.918d}{ab} \quad (5)$$

where M=3.06 is Taylor factor, G is the shear modulus of the Al matrix (26.2 GPa), b is the magnitude of Burgers vector of the Al matrix (0.286 nm), ν=0.33 represents Poisson's ratio[40]. f is the volume fraction of the precipitates. a=d/t represents the aspect ratio of the precipitates, where t and d are the thickness and diameter of the precipitates.

All parameters were substituted into Eq. (5), then the yield strength contribution from the Al_2Cu phase is 144 MPa, 113 MPa, 155 MPa, and 118 MPa for aging treatment of 175 °C/7 h, 175 °C/10 h, 120 °C/5 h+175 °C/5 h, and 120 °C/5 h+175 °C/8 h, respectively. In contrast, the yield strength contribution from the $Al_5Cu_2Mg_8Si_6$ phase is 39.2 MPa, 34.3 MPa, 45.3 MPa, and 41.7 MPa, respectively. These results indicate that the Al_2Cu phase provides a higher strengthening effect. Taking 175 °C/7 h as the reference (ΔYS=0), the experimental yield-strength changes for 175 °C/10 h, 120 °C/5 h+175 °C/5 h, and 120 °C/5 h+175 °C/8 h are −30.1 MPa, +5.5 MPa, and −12.3 MPa, respectively. The corresponding calculated changes in precipitation strengthening from Al_2Cu and $Al_5Cu_2Mg_8Si_6$ are −35.9 MPa, +17.1 MPa, and −23.5 MPa. The calculation captures the same sign and trend of ΔYS, indicating that the room-temperature yield-strength variation is mainly governed by precipitation strengthening from Al_2Cu and $Al_5Cu_2Mg_8Si_6$. The remaining discrepancy arises from

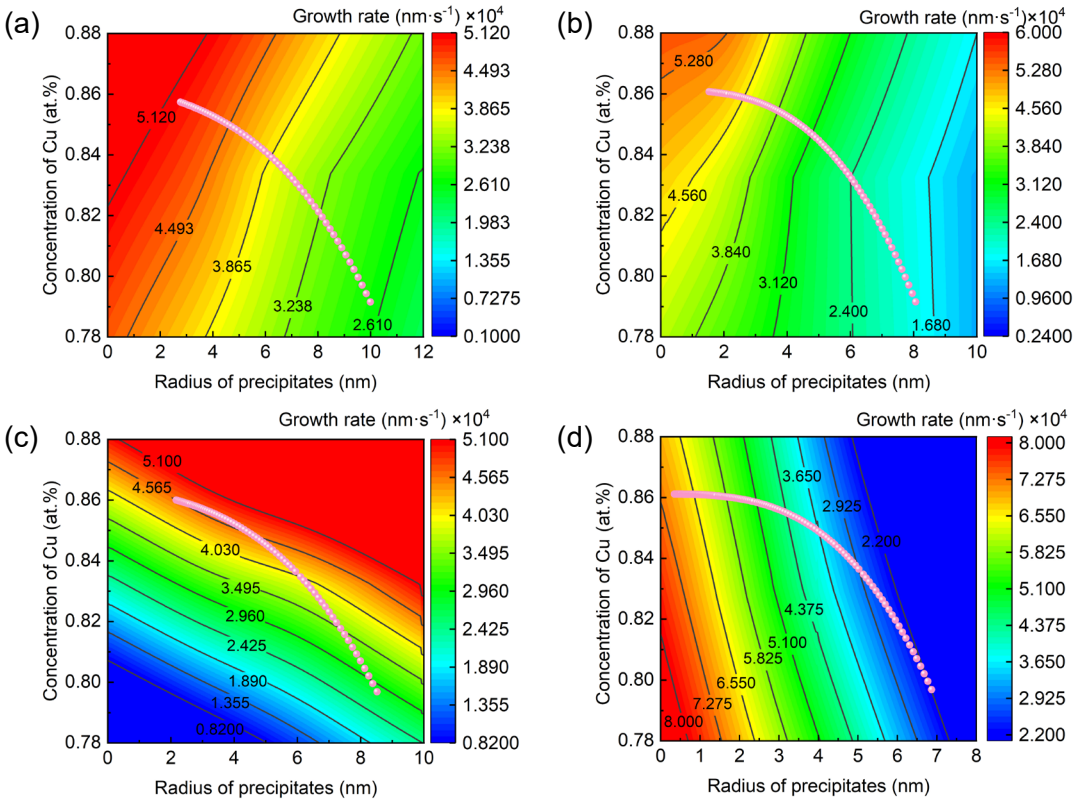

Fig. 10: Growth rate contour diagram of solid solution concentration with precipitation radius: (a) single-stage aging (175 °C/7 h)-Al_2Cu; (b) single-stage aging (175 °C/7 h)-$Al_5Cu_2Mg_8Si_6$; (c) double-stage aging (120 °C/5 h+175 °C/5 h)-Al_2Cu; (d) double-stage aging (120 °C/5 h+175 °C/5 h)-$Al_5Cu_2Mg_8Si_6$

strengthening contributions not included in the Orowan-based analysis (e.g., solid-solution, dislocation, and grain-boundary strengthening) and from idealizations in precipitate geometry.

5 Conclusions

Two different aging treatments were designed to investigate the effects of aging processes on the microstructures and mechanical properties of casting Al-8.5Si-2Cu-0.9Mg alloy. The optimal aging process for the alloy was identified. The key findings of the study are summarized as follows:

(1) The Al-8.5Si-2Cu-0.9Mg alloy consists of α-Al, Si, Al_2Cu, and $Al_5Cu_2Mg_8Si_6$ phases. Under the double-stage aging treatment, both the θ' and Q' (or alternatively, the θ'' and Q') phases are finer and more numerous than those formed under single-stage aging. In particular, the θ'' and Q' phases in the alloy aged at 120 °C/5 h+175 °C/5 h exhibit the smallest sizes, with the diameter and thickness of the θ'' phase measuring 17.98 nm and 1.54 nm, respectively, and the diameter of the Q' phase measuring 5.64 nm.

(2) At room temperature, the Al-8.5Si-2Cu-0.9Mg alloy at 120 °C/5 h+175 °C/5 h exhibits the highest tensile strength. At room temperature, the yield strength, ultimate tensile strength, and elongation of the alloy are 278.1 MPa, 359.4 MPa, and 3.1%, respectively. At the tensile temperature of 250 °C, the alloy aged at 120 °C/5 h+175 °C/8 h demonstrates the highest tensile strength and a better elongation, with yield strength of 174.2 MPa, ultimate tensile strength of 212.6 MPa, and an elongation of 7.2%.

(3) Theoretical calculations indicate that the nucleation rate of the $Al_5Cu_2Mg_8Si_6$ phase is higher than that of the Al_2Cu phase, and the number density of the Al_2Cu phase exceeds that of $Al_5Cu_2Mg_8Si_6$ phase. Furthermore, double-stage aging (120 °C/5 h+175 °C/5 h) significantly increases both the nucleation rate and the number density of the $Al_5Cu_2Mg_8Si_6$ and Al_2Cu phases. Under double-stage aging (120 °C/5 h+175 °C/5 h), the growth rates of the Al_2Cu and $Al_5Cu_2Mg_8Si_6$ phases are slightly lower than those observed under single-stage aging (175 °C/7 h).

Acknowledgment

This work was supported by the Key R&D Projects in Heilongjiang Province (GA23A901).

Conflict of interest

The authors declare that they have no conflicts of interest.

References

[1] Samuel E, Garza-Elizondo G H, Abdelaziz M H, et al. Effect of Mn, Ni, and Zr addition on the tensile properties and precipitation behavior of Sr-modified Al-Si-Cu-Mg-Based alloys. International Journal of Metalcasting, 2025, 19: 1741–1758.

[2] Godbol K, Bhushan B, Narayana M S V S, et al. Al-Si controlled expansion alloys for electronic packaging applications. Progress in Materials Science, 2024, 144: 101268.

[3] Wang X B, Rong L, Huang H, et al. Effect of Er, Zr and heat treatment on microstructure and mechanical properties of high zinc aluminum alloy. Rare Metal Materials and Engineering, 2024, 53(1): 250–256.
[4] Pereira C L, Gomes L F, Garcia A, et al. Comparing the roles of Sb and Bi on microstructures and application properties of the Al-15% Si alloy. Journal of Alloys and Compounds, 2021, 878: 160343.
[5] Zhang N, Feng Y C, Zhao S C, et al. Microstructure evolution and mechanical properties of Al-12Si-*x*Cu-*y*Ni-1Mg alloy with different Ni/Cu ratios. Materials Today Communications, 2024, 38: 108081.
[6] Zhang M S, Tian Y Q, Zheng X, et al. Research progress on multi-component alloying and heat treatment of high strength and toughness Al-Si-Cu-Mg cast aluminum alloys. Materials, 2023, 16(3): 1065.
[7] Yamamoto K, Takahashi M, Kamikubo Y, et al. Effect of Mg content on age-hardening response, tensile properties, and microstructures of a T5-treated thixo-cast hypoeutectic Al-Si alloy. Materials Science and Engineering: A, 2020, 798: 140089.
[8] Son H W, Lee J Y, Cho Y H, et al. Enhanced mechanical properties and homogeneous T5 age-hardening behavior of Al-Si-Cu-Mg casting alloys. Journal of Alloys and Compounds, 2023, 960: 170982.
[9] Cao Y D, Chen X Y, Wang Z D, et al. Effect of Cd micro-addition on microstructure and mechanical properties in ternary Al-Si-Cu alloy. Journal of Alloys and Compounds, 2021, 851: 156739.
[10] Cui X M, Cui H, Zhao X P, et al. Effects of heat treatment on microstructure, mechanical properties and corrosion resistance of Al-Si-Mg-3%Cr alloy. Rare Metal Materials and Engineering, 2023, 52(9): 3179–3185.
[11] Jiang Y H, Zheng H T, Liu F, et al. Strength and ductility optimization of HPDC $AlSi_8MgCuZn_2$ alloys by modifying pre-aging treatment. China Foundry, 2024, 21(1): 1–9.
[12] Chen Y, Hu Q, Pan S, et al. Influences of Cu content on the microstructure and strengthening mechanisms of Al-Mg-Si-*x*Cu alloys. Metals, 2019, 9(5): 524.
[13] Zheng Y, Xiao W L, Ge S J, et al. Effects of Cu content and Cu/Mg ratio on the microstructure and mechanical properties of Al-Si-Cu-Mg alloys. Journal of Alloys and Compounds, 2015, 649: 291–296.
[14] Beroual S, Boumerzoug Z, Paillard P, et al. Effects of heat treatment and addition of small amounts of Cu and Mg on the microstructure and mechanical properties of Al-Si-Cu and Al-Si-Mg cast alloys. Journal of Alloys and Compounds, 2019, 784: 1026–1035.
[15] Su R M, Jia Y X, Xiao J, et al. Effect of secondary aging on microstructure and properties of cast Al-Cu-Mg alloy. China Foundry, 2023, 20(1): 71–77.
[16] Lombardi A, Ravindran C, MacKay R. Optimization of the solution heat treatment process to improve mechanical properties of 319 Al alloy engine blocks using the billet casting method. Materials Science and Engineering: A, 2015, 633: 125–135.
[17] Zhu X, Dong X, Blake P, et al. Improvement in as-cast strength of high pressure die-cast Al-Si-Cu-Mg alloys by synergistic effect of Q-$Al_5Cu_2Mg_8Si_6$ and θ-Al_2Cu phases. Materials Science and Engineering: A, 2021, 802: 140612.
[18] Yuan Y, Sui Y, Zhu S, et al. Enhanced mechanical properties of as-cast Al-7.0Si-1.5Cu-*x*Mg alloys through synergistic main strengthening phases by controlling Mg element. Journal of Alloys and Compounds, 2024, 983: 173856.
[19] Andersen S J, Marioara C D, Friis J, et al. Precipitates in aluminium alloys. Advances in Physics: X, 2018, 3(1): 1479984.
[20] Kahlenberg R, Wojcik T, Falkinger G, et al. On the precipitation mechanisms of β-Mg_2Si during continuous heating of AA6061. Acta Materialia, 2023, 261: 119345.
[21] Fang N, Zou C M, Wei Z J, et al. Effect of Ge and Mg additions on the aging response behavior and mechanical properties of Al-Si-Cu alloy. Materials Science and Engineering: A, 2021, 811: 141024.
[22] Xue L W, Jia H L, Ma P K, et al. Influence of Mg and Cu on precipitation behaviors and mechanical properties of Al-Si alloys. Materials Science and Engineering: A, 2024: 146775.
[23] Dash S S, Chen D. A review on processing-microstructure-property relationships of Al-Si alloys: Recent advances in deformation behavior. Metals, 2023, 13(3): 609.
[24] Yao J Y, Taylor J A. Characterization of intermetallic particles formed during solution treatment of an Al-7Si-0.4Mg-0.12Fe alloy. Journal of Alloys and Compounds, 2012, 519: 60–66.
[25] Li R X, Li R D, Zhao Y H, et al. Age-hardening behavior of cast Al-Si base alloy. Materials Letters, 2004, 58(15): 2096–2101.
[26] Sjölander E, Seifeddine S. The heat treatment of Al-Si-Cu-Mg casting alloys. Journal of Materials Processing Technology, 2010, 210(10): 1249–1259.
[27] Zhang B R, Zhang L K, Wang Z M, et al. Achievement of high strength and ductility in Al-Si-Cu-Mg alloys by intermediate phase optimization in as-cast and heat treatment conditions. Materials, 2020, 13(3): 647.
[28] Xu C C, He H, Yu W Y, et al. Influence of quenching temperature on peak aging time and hardness of Al-Mg-Si-Cu alloys strengthened by nano-sized precipitates. Materials Science and Engineering: A, 2019, 744: 28–35.
[29] Zuo L J, Ye B, Feng J, et al. Effect of Q-$Al_5Cu_2Mg_8Si_6$ phase on mechanical properties of Al-Si-Cu-Mg alloy at elevated temperature. Materials Science and Engineering: A, 2017, 693: 26–32.
[30] Zhang M, Tian Y, Zheng X, et al. Research progress on multi-component alloying and heat treatment of high strength and toughness Al-Si-Cu-Mg cast aluminum alloys. Materials, 2023, 16(3): 1065.
[31] Li R X, Chen Y J, Yuan X G, et al. Effects of Cd and Sn on double-peak age-hardening behaviors of Al-Si-Cu-Mg cast alloys. China Foundry, 2010, 7(1): 1–5.
[32] Wang G Q, Bian X F, Qiao J G, et al. Effect of be on aging behavior of an Al-Si-Cu-Mg cast alloy. Journal of Materials Engineering and Performance, 2004, 13: 99–102.
[33] Zhao B B, Ye B, Wang L Y, et al. Effect of ageing and thermal exposure on microstructure and mechanical properties of a HPDC Al-Si-Cu-Mg alloy. Materials Science and Engineering: A, 2022, 849: 143463.
[34] Liao H, Wu Y, Ding K, et al. Hardening response and precipitation behavior of Al-7%Si-0.3%Mg alloy in a pre-aging process. Materials Science and Engineering: A, 2013, 560: 811–816.
[35] Aruga Y, Kozuka M, Takaki Y, et al. Effects of natural aging after pre-aging on clustering and bake-hardening behavior in an Al-Mg-Si alloy. Scripta Materialia, 2016, 116: 82–86.
[36] Zhen L, Kang S B, Kim H W. Effect of natural aging and preaging on subsequent precipitation process of an Al-Mg-Si alloy with high excess silicon. Materials Science and Technology, 1997, 13(11): 905–911.
[37] Shaha S K, Czerwinskl F, Kasprzak W, et al. Interaction between nano-precipitates and dislocations during high temperature deformation of Al-Si alloy. Journal of Alloys and Compounds, 2017, 712: 219–224.
[38] Deschamps A, Brechet Y. Influence of predeformation and ageing of an Al-Zn-Mg alloy-II. Modeling of precipitation kinetics and yield stress. Acta Materialia, 1998, 47(1): 293–305.
[39] Ji Y, Ghaffari B, Li M, et al. Phase-field modeling of θ' precipitation kinetics in 319 aluminum alloys. Computational Materials Science, 2018, 151: 84–94.
[40] Dash S S, Liu Z Y, Zou Y, et al. Strengthening mechanisms and work hardening in a heterostructured cast aluminum alloy under compressive loading: Correlation with nanomechanical properties. Journal of Alloys and Compounds, 2023, 968: 171844.